Supplementary Materials(SM)

This PDF file includes:

Materials and Methods
Figs. S1 to S9
References

Other Supporting Information Files:

Table S1 to S4 (Excel file)

Materials and Methods

1 General configurations

We follow Depoorter's paper (Depoorter et al., 2013) to define study regions over Antarctica for the six oceanic sectors, namely the Ross sea (ROS), Amundsen sea (AMU), Bellingshausen Sea (BEL), Weddell Sea (WED), West Indian Ocean (WIS), and East Indian Ocean (EIS). Minor adjustments are made to ensure that each ice basin defined by Zwally (Zwally, et al.,2012) is organized into a unique oceanic sector. For example, the Sulzberger catchment is adjusted to be in the Amundsen Sea sector while it is part of the Ross Sea sector in Depoorter's paper, and the Batch catchment is incorporated into Bellingshausen Sea sector instead of Amundsen Sea sector.

The grounding lines of the Antarctic ice sheet are obtained from a synthetic compilation of published grounding lines (Depoorter et al., 2013). Minor adjustments are made for calculating ice fluxes at different time periods due to incomplete ice thickness and ice flow data, for example, the grounding lines in Frost Glacier has moved inland about 2 km since 2006, and the partial grounding lines in Western Antarctic Peninsula (WAP) are adjusted, especially in the areas with fast-flowing glaciers. Furthermore, the other three data products of grounding lines, Antarctic Surface Accumulation and Ice Discharge (ASAID) (Bindschadler et al., 2011), InSAR (Rignot et al., 2011), and MOA(Bohlander and Scambos, 2007), are used in this study for uncertainty estimates of ice mass discharges due to the grounding-line migrations.

The Bedmap-2 ice thickness data along with ice penetrating radar (IPR) thickness from multiple campaigns from 2002 to 2014 are used to calculate the ice fluxes in combination with ice velocity vectors. The IPR data are from multiple radar sounder instrument in multi-campaigns from NASA's Operation IceBridge (OIB) project, including the Hi-Capability Radar Sounder (HiCARS) instrument(Blankenship et al.,

2011, 2012), and the Multichannel Coherent Radar Depth Sounder (MCorDS)(Allen, 2013, 2011).

The ice fluxes (ice mass discharges) are calculated for individual glaciers or ice streams. Because of as much as 74% of ice discharged through ice shelves and floating ice tongues (Bindschadler et al., 2011), and due to ice-shelf buttressing to ice-sheet flow, we investigate the potential linkage of ice dynamics between glaciers and ice shelves. Thus, all glaciers draining into the same ice shelf are treated as a whole in mass discharge estimates. For the complete survey of the ice fluxes, the ice fluxes across the grounding lines not fringed by ice shelves are also calculated in this study, while previous studies used extrapolation for non-surveyed area(Depoorter et al., 2013; Rignot et al., 2013) (Table S2). Additionally, all results are shown with 1-σ uncertainty.

2 Mass balance of the ice sheet

Surface mass balance (SMB, or surface snow accumulation) is dominated by precipitation (snowfall) in Antarctica. Here, we calculate the inflow mass (i.e. SMB) using new SMB data product (1979-2014)(van Wessem et al., 2014) at a horizontal resolution of 27.5 km in Antarctica except for the Peninsula, simulated by the regional Atmospheric Climate Model RACMO2.3 and a firn densification model (FDM)(Ligtenberg et al., 2011) for each of 27 glacier drainage basins (Zwally et al., 2012) (Fig. S1). In Antarctic Peninsula, we use a higher-resolution surface mass balance model over the time period 1979–2014, simulated by the regional atmospheric climate model RACMO2.3 and a firn densification model(van Wessem et al., 2016). The RACMO2.3 hydrostatic model runs at a horizontal resolution of ~5.5 km and 40 vertical levels, which is suitable for the Peninsula with sharp climate gradients and steep mountainous terrain(Lenaerts et al., 2014). The model combines the dynamics package of the High Resolution Limited Area Model (HIRLAM) with the physics package of the European Centre for Medium-range Weather Forecasts (ECMWF) Integrated Forecast System (IFS) (ECMWF-IFS, 2008)(van Wessem et al., 2014).

The SMB values are estimated on the 27 glacier drainage basins (Table S3). The total SMB of the Antarctic ice sheet is 1,901 Gt yr^{-1} with an interannual variability of 58 Gt yr^{-1}, which is similar to the newly published result by use of the same SMB product(van Wessem et al., 2014), and also comparable with previous study of 1,983±122 Gt yr^{-1}(Lenaerts et al., 2012). In the Antarctic Peninsula (AP), West Antarctica (WA) and East Antarctica (EA), SMB values account for 12%, 30% and 58% of the values for the entire Antarctic ice sheet, respectively, and the snow accumulation rates per unit area are 939 mm yr^{-1}, 330 mm yr^{-1}, and 111 mm yr^{-1}, respectively. The mean accumulation rate on the entire ice sheet is 160 mm yr^{-1}.

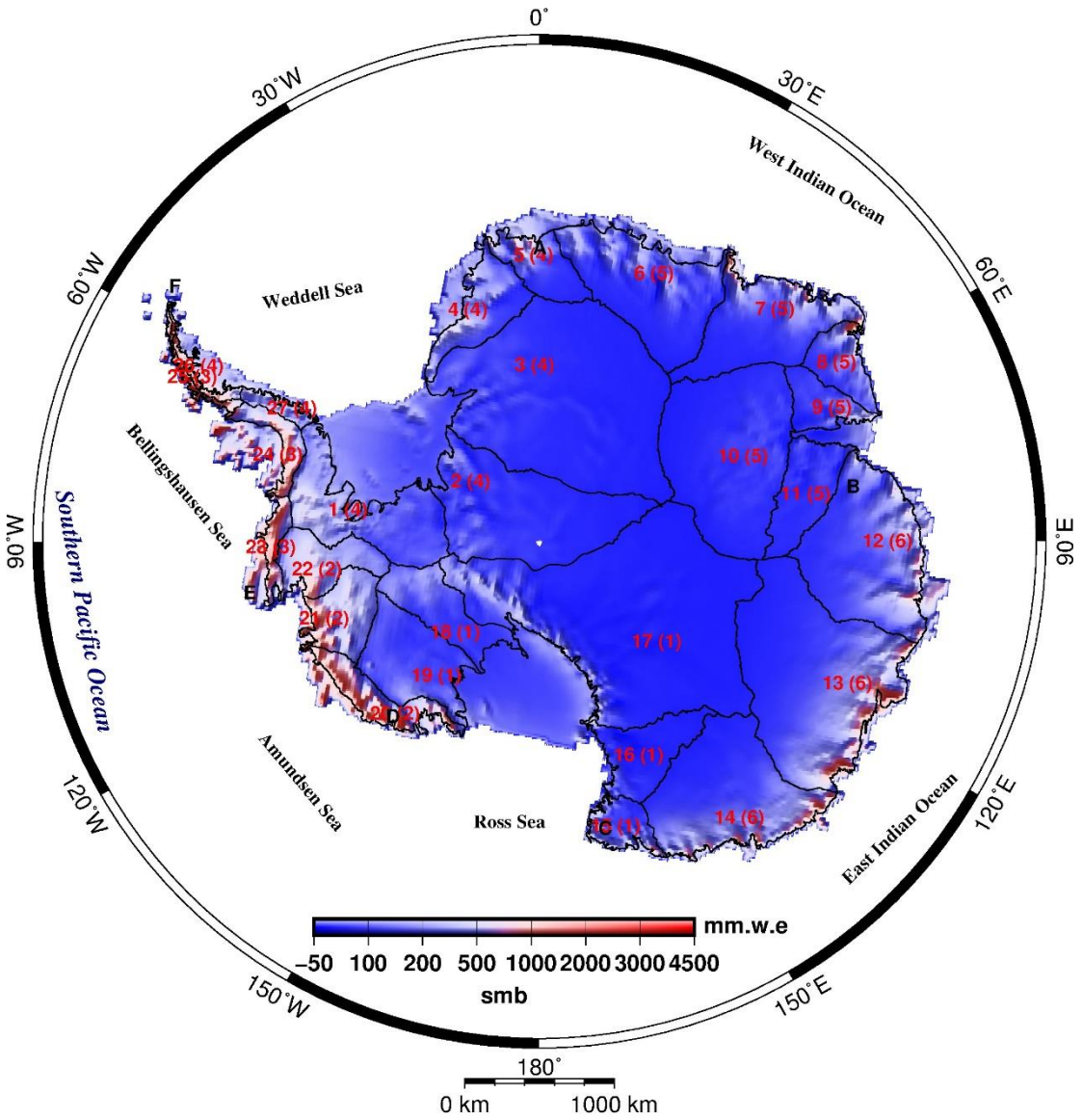

Figure S1. The SMB is an average of snow accumulation from 1979 to 2014 simulated by the RACMO2.3(van Wessem et al., 2014) and the FDM model(Ligtenberg et al., 2011). The magnitude of SMB is colour-coded (in mm yr^{-1} water equivalent). The grounded ice sheet is overlain by the major basins (divided by black solid lines). Basins and the affiliated oceanic sector are denoted by numbers and the accompanied numbers in parentheses. 1. Ross Sea (ROS); 2. Amundsen Sea (AMU); 3. Bellingshausen Sea (BEL); 4. Weddell Sea (WED); 5. West Indian Ocean (WIS); and 6. East Indian Ocean (EIS).

The mass discharge across each grounding line is calculated with the rigorous flux gate method (Rignot et al., 2013), in combination with ice velocity and Bedmap-2 ice thickness associated with IPR track measurements between 2002 and 2014 from Operation IceBridge (OIB) project (Table S2). Our procedure can integrate ice flux along the grounding line pixel-by-pixel with the consideration of the directions of ice

velocity vector and grounding line. The total mass discharges across grounding lines in Antarctica are 2,082±37 Gt yr^{-1}, 2,133±16 Gt yr^{-1} and 2,131±16 Gt yr^{-1} in 2006, 2014 and 2015 respectively. Our estimates in 2006 is the same as recently published estimates (Depoorter et al., 2013; Rignot et al., 2013). It should be noted that the mass balance in Bellingshausen Sea sectors is more likely underestimated because the mass discharge through the surface meltwater in summer due to high air temperature above freezing point, is not taken into account. Negative ice flux of estimates are found in four small glaciers, which is more likely caused by geolocation error of grounding lines or the uncertainty of ice velocity, but have no effect on the resulting mass balance estimates for the entire Antarctica.

3 Uncertainty

3.1 The uncertainty of SMB

For each SMB grid in Antarctica (excluding ice shelves), we fit a trend and the coefficients associated with seasonal periodicities using the least squares method to the monthly time series of accumulated SMB data. The standard deviation for the trend can be used as the uncertainty of the SMB. The uncertainties for the contained grids are simply summed to give the uncertainty for the whole Antarctic ice sheet, and the uncertainties for 27 glacier basins respectively. For the six oceanic sectors, the uncertainties of corresponding glacier basins are totalized to give the SMB uncertainty estimate. All the SMB uncertainties can be found in Tables 1 and S2. The total uncertainty of the SMB is ±58 Gt yr^{-1} for the entire Antarctic ice sheet.

3.2 The uncertainty of ice discharge

3.2.1 Method

In the process of calculating ice discharge across a grounding line, the grounding line is divided into K segments, thus the uncertainty of the ice discharge (denoted σ_{GLF}) can be estimated using the following error propagation equation:

$$\sigma_{\mathrm{GLF}}^2=\sum_{k=1}^{K}\Delta m_k^2\left(\frac{\sigma_V}{V}\right)^2+\sum_{k=1}^{K}\Delta m_k^2\left(\frac{\sigma_T}{T}\right)^2+\sigma_G^2 \quad (4)$$

where Δm_k is the ice discharge across the k-th segment, the two k-th terms together denote the variance contributions from the k-th segment, σ_V and σ_T denote the uncertainties of the ice velocity (V) and ice thickness (T) in the k-th segment, and σ_G^2 is the variance contribution of the positioning error of the ground line; σ_V is estimated in main text, σ_T and σ_G are estimated in Sections 3.2.2, 3.2.3, respectively.

3.2.2 Uncertainty of ice thickness (σ_T)

The uncertainties of the ice thickness are obtained by Bedmap-2(Fretwell et al.,

2012; Fretwell et al., 2013). If the thicknesses are measured by radar and seismic techniques, the uncertainties are usually less than ±51.2 m, but if the thicknesses are derived from altimetry data under the assumption of hydrostatic equilibrium, the uncertainties are usually between ±100 m and ±150 m. The absolute errors of IPR data are variable according the type of instruments, the absolute errors are ±44.5m for MCorDS (Allen, 2013) and ±10 m for HiCARS (Young et al., 2011).

3.2.3 Ice flux uncertainty due to grounding-line positioning error (σ_G)

Mass change caused by migration of grounding line is still a challenge due to instrumentation difficulties in ice-choked fjords several hundred meters below the sea level(Joughin et al., 2012). Here, we use four data sets for grounding lines (from Antarctic Surface Accumulation and Ice Discharge, or ASAID(Bohlander and Scambos, 2007), InSAR(Rignot et al., 2008), DEP(Depoorter et al., 2013) and MOA(Bohlander and Scambos, 2007)) to calculate the ice discharge for Antarctic ice sheet. ASAID used Landsat-7 imagery and ICESat laser altimetry data obtained between 1999 and 2003 at 15 m resolution; InSAR data include data from the Earth Remote Sensing Satellite 1/2 (ERS-1/2), ALOS, PALSAR and RADARSAT-1/2 satellites, from 1994 to 2009; DEP used InSAR, ICESat altimeter and ASAID image data; and MOA grounding lines were determined by the Mosaic of Antarctica.

The ice discharges are respectively calculated with the flux gate method using the grounding line data from the above mentioned four data sources, together with the ice velocity data in 2006 and ice thickness data from Bedmap-2. The ice discharge uncertainties due to the grounding-line positioning errors are computed as one half of the maximal differences between the four estimates of the ice discharge. The total ice discharges in Antarctica corresponding to the four data sets are 2,078 Gt yr^{-1}, 2,048 Gt yr^{-1}, 2,007 Gt yr^{-1} and 2,029 Gt yr^{-1} respectively. Note that the value 2,048 Gt yr^{-1} is adopted from a recently published study[39] for the InSAR grounding lines. In summary, the uncertainty of the total ice discharge due to the grounding-line positioning error is ±31 Gt yr^{-1}.

4 Glacier dynamics

4.1 Ross Sea

Glaciers in Ross ice shelf. In Siple Coast (Fig. S2), the Bindschadler glacier (formerly called Ice Stream D), and other two unnamed glaciers closer to Ross Sea decelerated by more than 7% and up to 11% between 2015 and 2006, while the MacAyeal ice stream shows no significant change. It is noted that our measurements do not cover the Kamb, Whillans, and Van der Venn glaciers in the Siple Coast. The mass discharge in Siple coast during the last 10 years show no significant change at 0.3 Gt yr^{-1}. In the Transantarctic Mountains, the Marsh glacier shows fast acceleration

by 16%, however the largest Byrd glacier shows deceleration by about 7% from 2006 to 2015, and by 15% compared with earlier measurements in 1978(Brecher, 1982, 1986). To the north of the Byrd glacier, the Mulock glacier shows no significant change. The mass discharge in Transantarctic Mountains (basin 17) also shows no obvious change from 2006 to 2015.

Glaciers in Victoria Land. Ice dynamics of the glaciers shows apparent contrasting behavior. Those small size glaciers exhibit widespread accelerations from 3% to 166%, for example, the most rapid acceleration occurs in the Amos glacier (166%), Irving glacier (35%), and Suter glacier (50%) during the last decade. However, the larger glaciers exhibit primarily decelerations. For instance, the David glacier draining into the Drygalski ice shelf shows apparent slowdown by 21%, and Mariner glacier decelerates by 15%. In addition, there are also some glaciers show no significant change, such as Aviator, Borchgrevink, Tucker, and other unnamed small glaciers. The distinct contrasting behaviors in Victoria Land lead to no significant mass change in the area.

Glaciers in Gorge V Land. The majority of the glaciers in George V Land show acceleration from 8% to 181%. The large Rennick glacier accelerates by 19%, the small Crume and O'Hara glaciers show acceleration of 167% and 181%, an unnamed glacier shows the highest acceleration of 605%. Only two glaciers show slight deceleration of 4% in Noll and 11% in an unnamed glacier.

The apparent difference of ice dynamics in Victoria Land (basin 15,16) and George V Land (basin 15) as compared with Ross ice streams may be caused by warmer CDW which has been intruding the cavities in the grounding lines(Pritchard et al., 2012), while the Ross ice streams are not affected because of relatively colder subglacial environment due to colder ice-shelf meltwater from the larger Ross ice shelf.

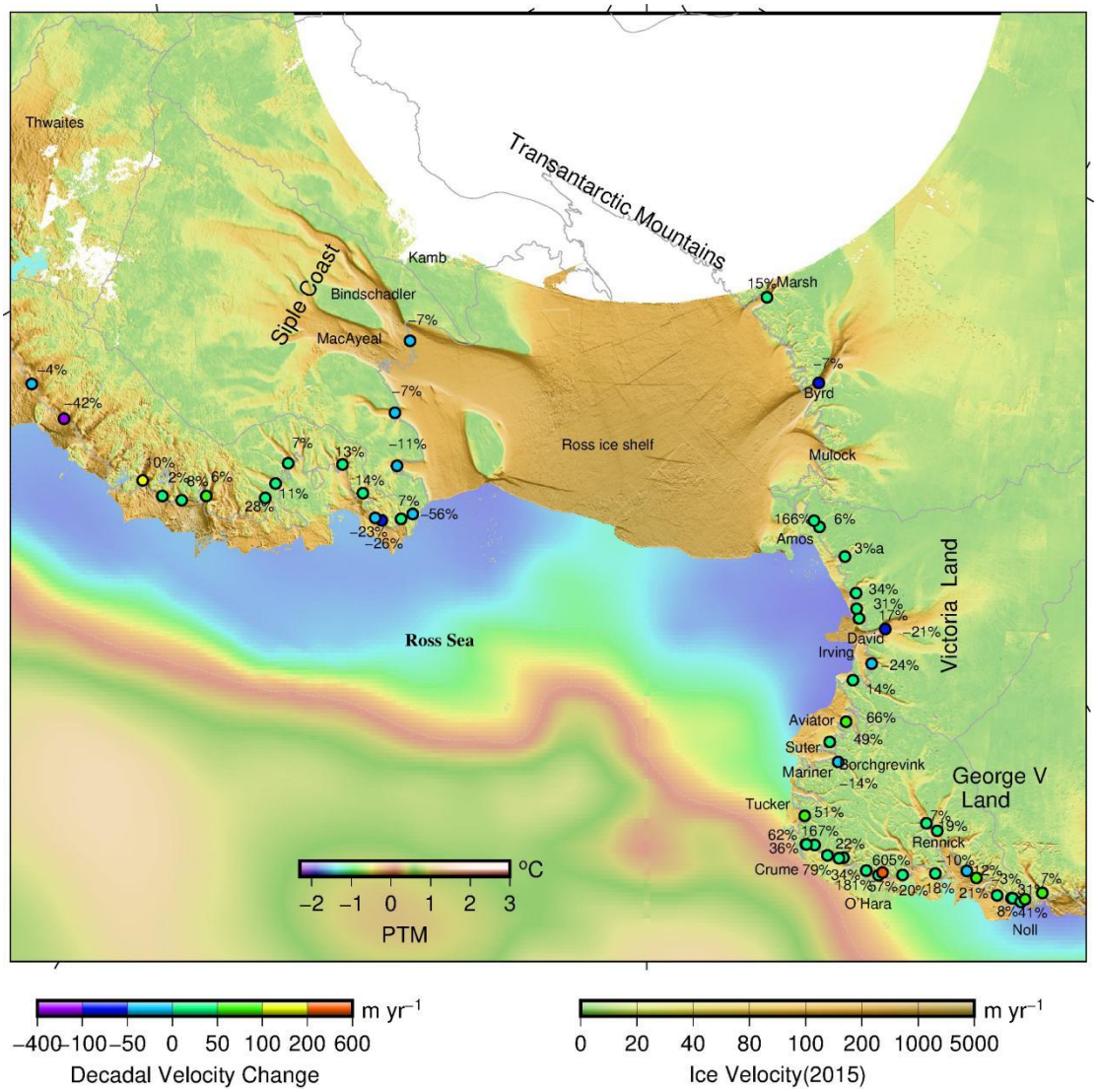

Figure S2. The ice velocity change between 2015 and 2006 in the Ross Sea sector, the color dots show the magnitudes of decadal velocity changes and the numbers stand for percent differences of velocities in 2015 with respect to 2006. The places and glaciers stated in the text are labeled. The ice velocity is color-coded on a logarithmic scale and overlaid on a gridded potential temperature data of seawater (PTM) at 200 m depth from the World Ocean Circulation Experiment (WOCE). Grey lines delimit the glacier basins and the grounding lines.

4.2 Amundsen Sea

Glaciers draining into Sulzberger ice shelf (Fig. S3) show an accelerated flow of 10% on average, which directly leads to accelerated mass discharge of 2.8 Gt yr^{-1} between 2015 and 2006. The Balchen glacier accelerates by 29% and Land glacier also shows an acceleration of 6%. However, in Getz ice shelf, as the largest ice shelf in the Amundsen Sea, its tributary glaciers show significant deceleration from 5% to 42%. Their slowdowns depicts an obvious deceleration of ice discharge (4.5 Gt yr^{-1}) from 2006 to 2015. The Kohler glacier in the Dotson ice shelf decelerates at 14%. However,

the Pine island Thwaites and Crosson glaciers show significant acceleration at 15%, 17% and 5%, respectively. The speedup in the Pine island glacier leads an accelerated mass discharge of 3 Gt yr^{-1} towards the Pine island ice shelf between 2015 and 2006. The Thwaites glacier speedup also contributes a significant accelerated mass discharge of 10.6 Gt yr^{-1}. The rapid acceleration of mass discharge in the Pine Island and Thwaites catchments cannot be totally explained by atmospheric condition. The oceanic thermocline condition may be one of the main factors result in the difference of ice dynamics, because the warmer CDW intrusion has been confirmed by Conductivity-temperature-depth(CTD) observations(Jacobs et al., 2011; Nakayama et al., 2013). Additionally, rapid basal melting and thinning in adjacent ice shelves are likely the other main factors leading to the ice flow acceleration(Nakayama et al., 2013) due to reduction or loss of buttressing force from ice shelves(Thomas et al., 2004). We also found the accelerated mass discharge estimates to be 13±1 Gt yr^{-1} during the last decade, 2006–2015, declining from 46±5 Gt yr^{-1} a decade earlier, 1996–2006(Rignot et al., 2008).

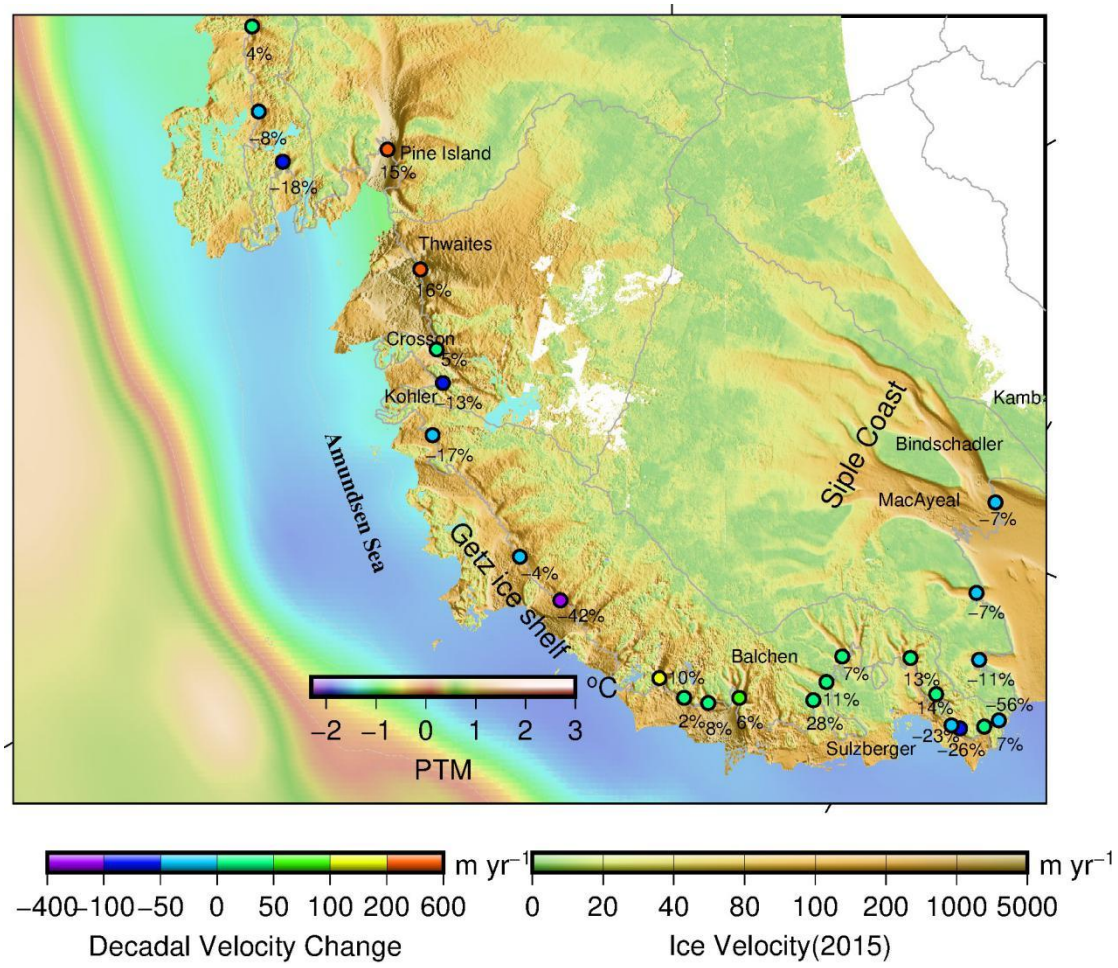

Figure S3. Same as Figure S2, but in the Amundsen Sea sector

There are multiple observations of ice velocity in the Pine Island glacier (Fig. S4)

and the Thwaites glacier (Fig. S5), and their ice shelves since 1996(Scheuchl, 2013), which allows us to investigate ice dynamics over a longer time period. Here, we investigate the profiles along the ice flow central line from upstream ice streams to ice shelves. Both Pine Island glacier and its ice shelf show a progressive simultaneous acceleration, the higher acceleration occurred during two decades ago (1996-2006), than the last decade (2006–2015). The slowdown of acceleration may either suggest a sign of cease of the episode of fast retreat or a short-lived decrease of acceleration(Hillenbrand et al., 2013). The current dynamics of the glacier seems to be controlled by the ice-shelf dynamics because of the synchronous changes of glacier and ice shelf, and increasing meltwater production beneath the ice shelf(Jacobs et al., 2011; Jenkins et al., 2010). Thwaites glacier shows similar ice dynamics, but the temporal pattern of ice velocity is distinctly different. The velocities of the glacier and ice shelf increased suddenly in 2005 and then remained stable until now, and the acceleration seems to affect only upstream 20 km from grounding line. The significant difference between upstream and downstream of the glacier probably attributes the special bathymetry configuration, in which there is a relative high ridge in upstream 20 km off the grounding line, and the warmer CDW probably may not yet invade the upstream of the ridge. However, in the Pine Island glacier, the acceleration in upstream 200km off the grounding line can be still found, which is caused by a seaward sloping bed in the upstream, and the warmer CDW probably has been intruding into the inland sloping bed in the vicinity of grounding line. The differential bathymetry configurations likely lead to distinct dynamic patterns in the adjacent two glaciers, although subjecting to the same atmospheric and oceanic forcing.

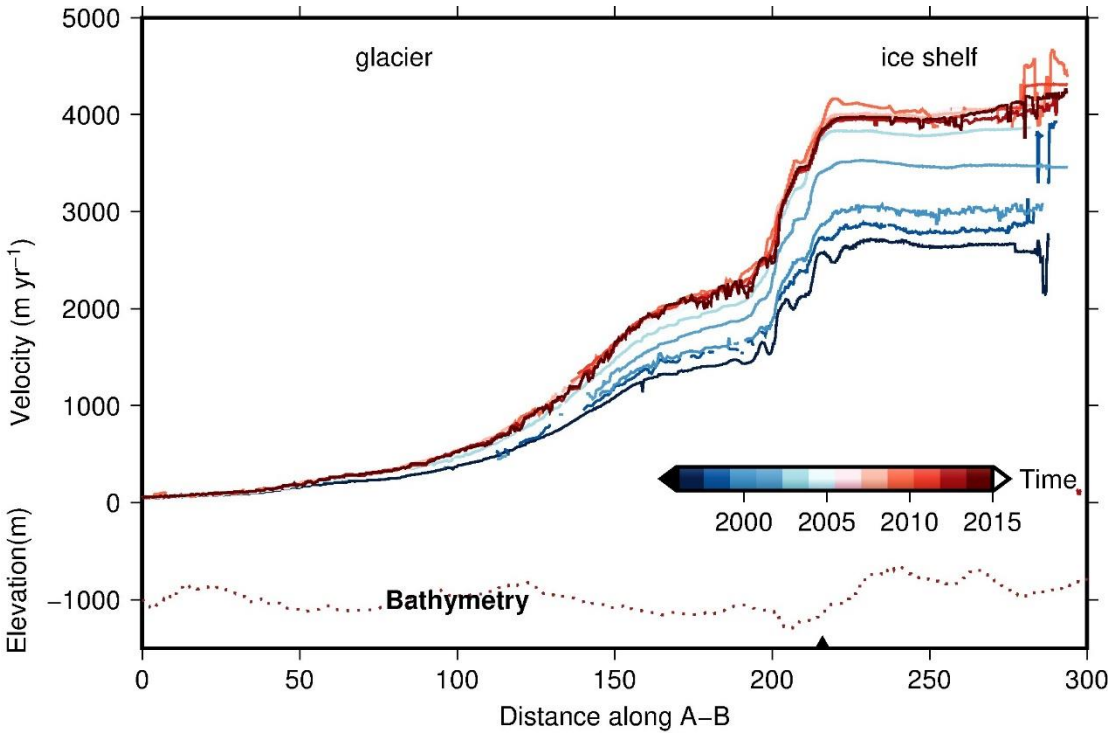

Figure S4. Ice dynamics in the Pine Island glacier and its ice shelf. The dotted line shows the bathymetry topography and black triangle indicates the location of grounding line. The ice velocity curves in entire surveyed period are color-coded by acquisition dates.

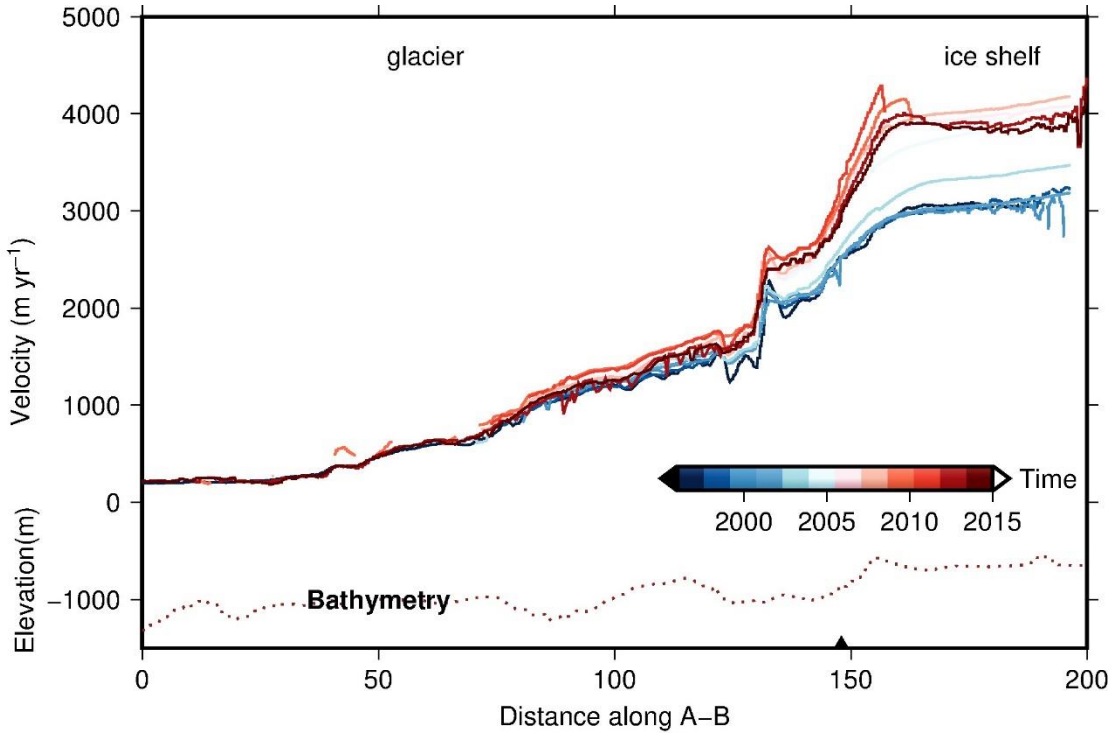

Figure S5. Same as Figure S4, but for the Thwaites glacier and its ice shelf.

4.3 Bellingshausen Sea

In the Antarctic Peninsula, the largest acceleration occurred in the small glaciers. The 2015 ice velocities are as much as 18-fold the velocity in 2006 (Fig. S6, Table S1), causing an accelerated mass discharge of 11±0.1 Gt yr^{-1}. The accelerated mass discharge is attributed more likely to warmer CDW which has been intruding into the cavity of these glaciers, and the significant increase of air temperature in Antarctic Peninsula (Cook et al., 2005; Hulbe et al., 2008; Martinson et al., 2008; Rignot et al., 2004; Vaughan et al., 2003). In the Wordie ice shelf, the Airy glacier draining into the ice shelf shows a velocity speedup of 70% from 2006 to 2015. The Airy glacier and the two unnamed glaciers in the ice shelf contribute the largest total accelerated mass discharge (~10 Gt yr^{-1}) in the Peninsula. However, the glaciers draining into George VI shelf show no significant accelerated mass discharge. Furthermore, the glaciers drainage into the large Abbot, Venable ice shelves show obvious decelerated mass discharges of 5.4 Gt yr^{-1} and 1 Gt yr^{-1}, respectively. It should be noted that the grounded glaciers directly interacting with warmer CDW also show accelerated mass discharges, such as the grounded glaciers near the Ferrigno ice shelf.

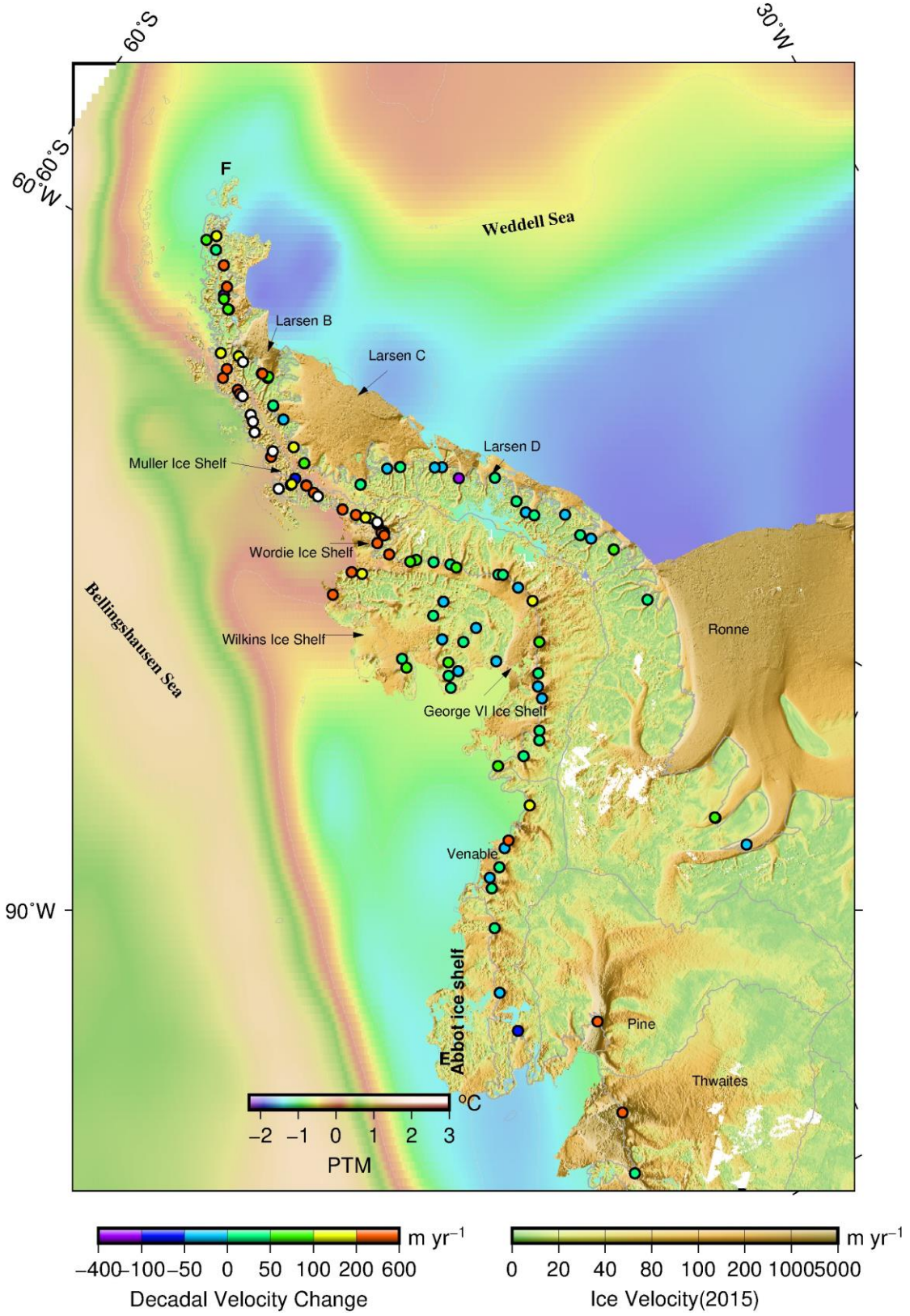

Figure S6. Same as Figure S2, but in the Antarctic Peninsula. The white-filled dots show that the changes are larger than 600 m yr^{-1}.

4.4 Weddell Sea

The Ronne-Filchner catchment (Fig. S7) shows an apparent accelerated mass discharge (7±11 Gt yr^{-1}) contributed vastly by glacier acceleration of Ketchum (by 11%) and another unnamed glacier (by 56%) flowing into Ronne ice shelf, although some glaciers in Ronne catchment also show deceleration, such as Evans glacier. Note that in Filchner catchment, there is no significant change in mass discharge (0.6±5 Gt yr^{-1}).

In the Brunt and Riiser catchment (basin 4), a significant accelerated mass discharge (6±2 Gt yr^{-1}) is found to be caused by widespread acceleration of the glaciers (Fig. S11, Table S2). For example, the Stancomb-Wills glacier flowing into Brunt ice shelf accelerated by 5.5% in velocity in the last decade. The Veststraumen glacier draining into Riiser ice shelf also shows an acceleration of 4%.

The widespread decelerated flow of glaciers draining into the Quar, Ekstrom, Atka, Jelbart and Fimbul ice shelves in basin 5 directly led to a total mass gain of near 4 Gt yr^{-1} during the last 10 years. For example, the Jutulstrauen glacier decelerated by 3% during the surveyed period. The Balakirev glacier draining into Jelbart ice shelf decelerated by 47%. As stated above, the glaciers in Coasts Land (basin 4) show accelerated discharge and the glaciers in Dronning Maud Land (basin 5) predominately show decelerated discharge.

In the eastern Antarctic Peninsula (EAP) (see Fig. S6), the glaciers in the Larsen B ice shelf show an accelerated mass discharge of 9% since 2006, The Talev glacier is found to be stagnant in 2006, but it shows a very large velocity of 1200 m yr^{-1} in 2015. Other glaciers in Larsen B ice shelf catchment accelerated by 20–70%. The fast motion and accelerated flows were found in the glaciers in Larsen B may be linked to the abrupt disintegration of the Larsen B ice shelf in March 2002, due to the loss of buttressing force from the ice shelf (Rignot et al., 2004; Scambos et al., 2004). Another region with a rapid accelerated discharge of up to 100% is the catchment surrounding Larsen A ice shelf, which broke off in 1995. Majority of other glaciers in EAP also show apparent accelerated flow, similar to the observation from altimetry since 2009 (Wouters et al., 2015). Compared with EAP, the acceleration of the glaciers in the WAP is more significant, caused predominately by oceanic driving mechanism(Wouters et al., 2015) and warmer air temperature(Hulbe et al., 2008), while the east coast is governed by cold oceanic conditions in the Weddell sea and obstacles of high mountains. The glaciers in Weddell Sea sector situated in East Antarctica show the dramatic difference of ice dynamics.

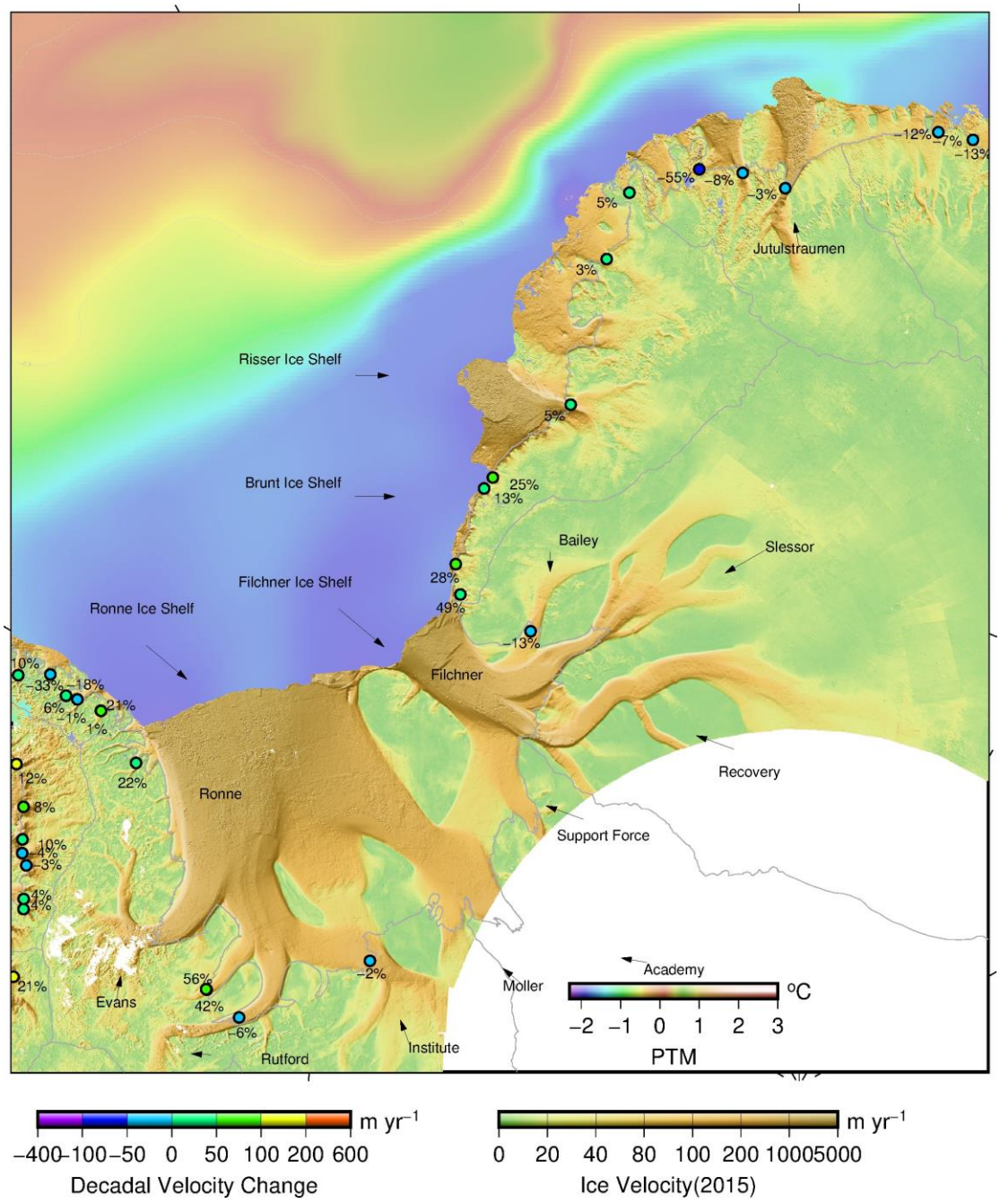

Figure S7. Same as Figure S2, but in the Weddell Sea

4.5 West Indian Ocean

The accelerated mass discharge is found in Enderby Land, mainly due to the speed up of glaciers in the area, such as the Robert, Wilma, Edward glaciers toward Edward WIII Bay, and Rayner and Thyer glaciers toward the Casey Bay (Fig. S8). In the Dronning Maud Land, to the west of Enderby Land, much of glaciers have undergone decelerated discharge from 2006 to 2015, especially for Shirase, Jutulstraumen glaciers with deceleration of 18% and 10% in mass discharge, respectively. In the Amery system, three largest Lambert, Mellor and Fisher glaciers also show slight

deceleration of –1%, –2%, –2% in velocities, respectively, which leads directly to a slight deceleration of mass discharge (–3 Gt yr^{-1}) from 2006 to 2015.

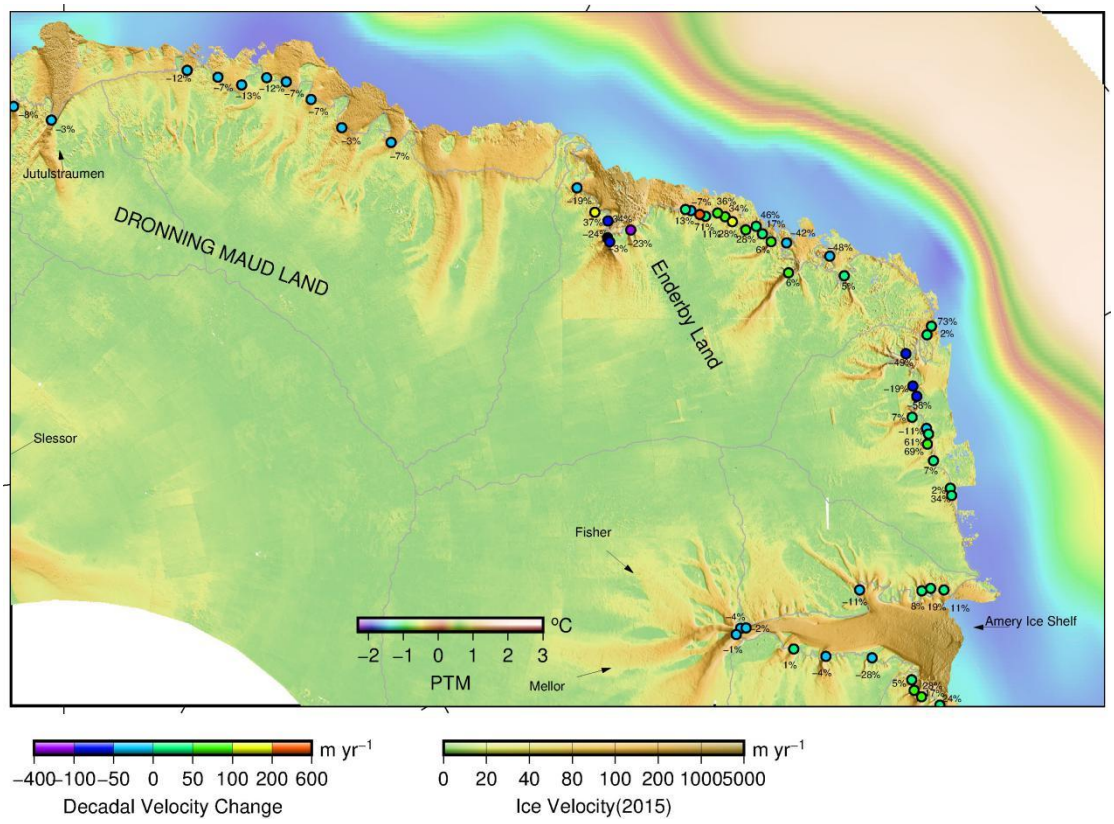

Figure S8. Same as Figure S2, but in the West Indian Ocean

4.6 East Indian Ocean

In the Wilkes Land, the accelerated mass discharges in all basins of the sector are observed (Fig. S9). The accelerated mass discharges are 10±3 Gt yr^{-1} for basin 12, 17±6 Gt yr^{-1} for basin 13, and 12±2 Gt yr^{-1} for basin 14, respectively. The accelerated losses in these glacier basins associated with similar bathymetry configuration to the West Antarctic ice sheet (Mengel and Levermann, 2014) , newly found trough beneath Totten glacier (Cook et al., 2013; Young et al., 2011) (Fig. 6), and potential CDW intrusion (Greenbaum et al., 2015), may eventually lead to the destabilization of the marine low-lying region, which also suggests a risk of the instability of the ice sheets in East Indian Ocean in the future.

In ASB (basin 13), the Moscow catchment decelerated by 5% in mass discharge between 2015 and 2006, while the Totten catchment accelerated by 2%, The difference probably results from local oceanic conditions, such as thickening in Moscow and thinning in Totten probably driven by ocean-forced instabilities (Aitken et al., 2016).

The WSB (basin 14), which holds ice more than five times that of West Antarctica (Mengel and Levermann, 2014), also shows an evident accelerated mass discharge

(12 Gt yr^{-1}), which is consistent with recent published study using altimetry measurements (McMillan et al., 2014). The majority of the glaciers in the area accelerate while some large glaciers remains stable or in decline, such as Cook.

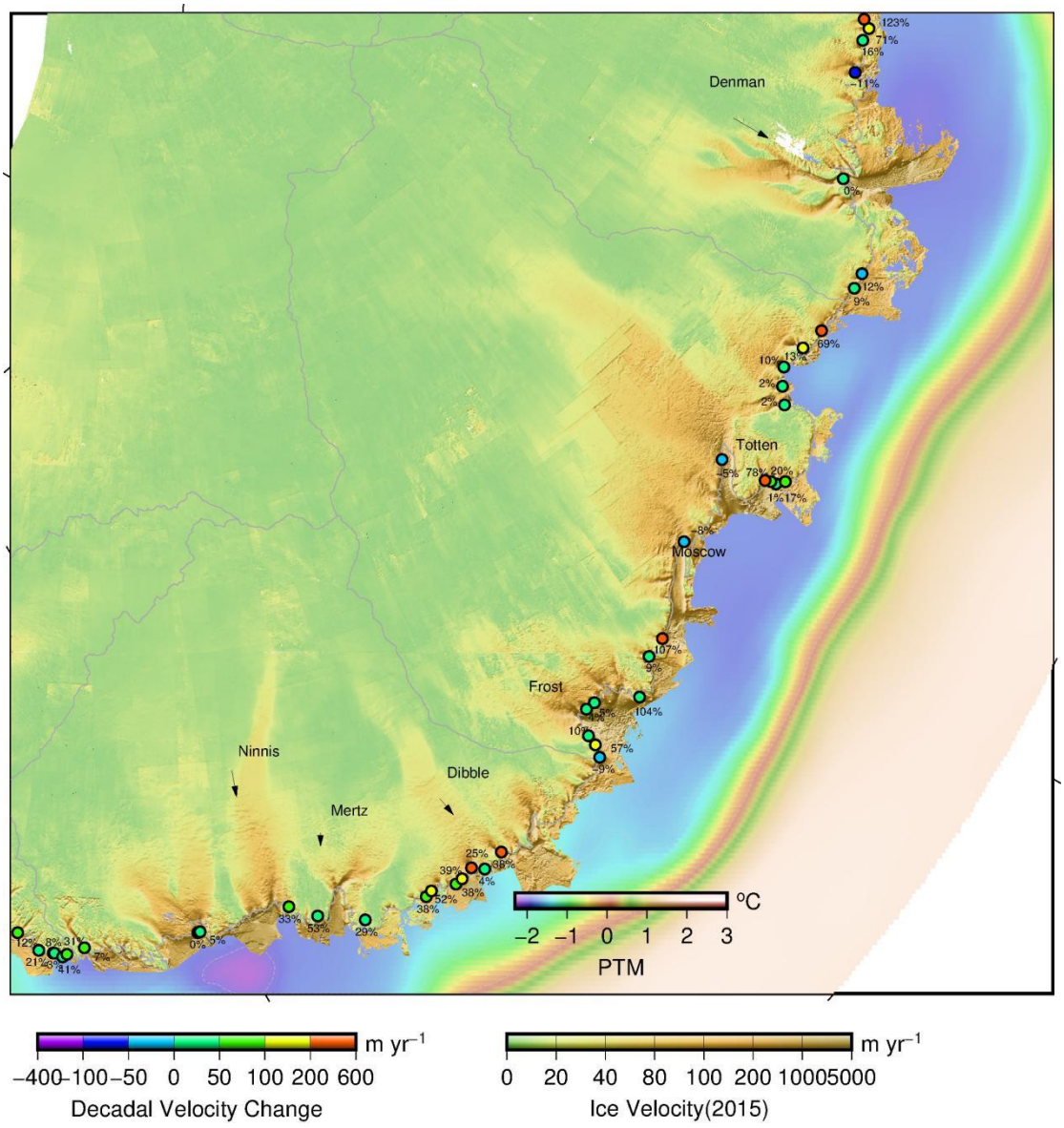

Figure S9. Same as Figure S2, but in the East Indian Ocean

References

Aitken, A. R. A., Roberts, J. L., Ommen, T. D. v., Young, D. A., Golledge, N. R., Greenbaum, J. S., Blankenship, D. D., and Siegert, M. J.: Repeated large-scale retreat and advance of Totten Glacier indicated by inland bed erosion, Nature, 533, 385-389, 2016.

Allen, C.: IceBridge MCoRDS L3 Gridded Ice Thickness, Surface, and Bottom, Version 2 In: IceBridge MCoRDS L3 Gridded Ice Thickness, Surface, and Bottom, Version 2, NASA DAAC at the

National Snow and Ice Data Center, Boulder, Colorado USA, 2013.
Allen, C.: Pre-IceBridge MCoRDS L2 Ice Thickness, Version 1. In: Pre-IceBridge MCoRDS L2 Ice Thickness, Version 1, NASA National Snow and Ice Data Center Distributed Active Archive Center, Boulder, Colorado USA, 2011.
Bindschadler, R., Choi, H., Wichlacz, A., Bingham, R., Bohlander, J., Brunt, K., Corr, H., Drews, R., Fricker, H., Hall, M., Hindmarsh, R., Kohler, J., Padman, L., Rack, W., Rotschky, G., Urbini, S., Vornberger, P., and Young, N.: Getting around Antarctica: new high-resolution mappings of the grounded and freely-floating boundaries of the Antarctic ice sheet created for the International Polar Year, Cryosphere, 5, 569-588, 2011.
Blankenship, D., Kempf, S., and Young, D.: IceBridge HiCARS 1 L2 Geolocated Ice Thickness Version 1.0. In: NASA Distributed Active Archive Center (DAAC) at the National Snow and Ice Data Center (NSIDC), NASA National Snow and Ice Data Center Distributed Active Archive Center, 2011.
Blankenship, D., Kempf, S., and Young, D.: IceBridge HiCARS 2 L2 Geolocated Ice Thickness, Version 1. In: Boulder, Colorado USA. NASA National Snow and Ice Data Center Distributed Active Archive Center, 2012.
Bohlander, J. and Scambos, T.: Antarctic coastlines and grounding line derived from MODIS Mosaic of Antarctica (MOA). Center, N. S. a. I. D. (Ed.), National Snow and Ice Data Center, Boulder, Colorado USA, 2007.
Brecher, H.: Photographic determination of surface velocities and elevations on Byrd Glacier, Antarctic Journal of the United States, 17, 79-81, 1982.
Brecher, H.: Surface velocity determination on large polar glaciers by aerial photogrammetry, Ann. Glaciol, 8, 22-26, 1986.
Cook, A., Fox, A., Vaughan, D., and Ferrigno, J.: Retreating glacier fronts on the Antarctic Peninsula over the past half-century, Science, 308, 541-544, 2005.
Cook, C. P., Flierdt, T. V. D., Williams, T., Hemming, S. R., Iwai, M., Kobayashi, M., Jimenez-Espejo, F. J., Escutia, C., González, J. J., and Khim, B. K.: Dynamic behaviour of the East Antarctic ice sheet during Pliocene warmth, Nature Geoscience, 6, 1-5, 2013.
Depoorter, M. A., Bamber, J. L., Griggs, J. A., Lenaerts, J. T., Ligtenberg, S. R., van den Broeke, M. R., and Moholdt, G.: Calving fluxes and basal melt rates of Antarctic ice shelves, Nature, 502, 89-92, 2013.
Fretwell, P., Pritchard, H., Vaughan, D., Bamber, J., Barrand, N., Bell, R., Bianchi, C., Bingham, R., Blankenship, D., and Casassa, G.: Bedmap2: improved ice bed, surface and thickness datasets for Antarctica, The Cryosphere Discussions, 6, 4305-4361, 2012.
Fretwell, P., Pritchard, H. D., Vaughan, D. G., Bamber, J. L., Barrand, N. E., Bell, R., Bianchi, C., Bingham, R. G., Blankenship, D. D., and Casassa, G.: Bedmap2: improved ice bed, surface and thickness datasets for Antarctica, Cryosphere, 7, 375-393, 2013.
Greenbaum, J., Blankenship, D., Young, D., Richter, T., Roberts, J., Aitken, A., Legresy, B., Schroeder,

D., Warner, R., and van Ommen, T.: Ocean access to a cavity beneath Totten Glacier in East Antarctica, Nature Geoscience, 8, 294-298, 2015.

Hillenbrand, C. D., Kuhn, G., Smith, J. A., Gohl, K., Graham, A. G. C., Larter, R. D., Klages, J. P., Downey, R., Moreton, S. G., Forwick, M., and Vaughan, D. G.: Grounding-line retreat of the West Antarctic Ice Sheet from inner Pine Island Bay, Geology, 41, 35-38, 2013.

Hulbe, C. L., Scambos, T. A., Youngberg, T., and Lamb, A. K.: Patterns of glacier response to disintegration of the Larsen B ice shelf, Antarctic Peninsula, Global Planet. Change, 63, 1-8, 2008.

Jacobs, S. S., Jenkins, A., Giulivi, C. F., and Dutrieux, P.: Stronger ocean circulation and increased melting under Pine Island Glacier ice shelf, Nature Geosci., 4, 519-523, 2011.

Jenkins, A., Dutrieux, P., Jacobs, S. S., McPhail, S. D., Perrett, J. R., Webb, A. T., and White, D.: Observations beneath Pine Island Glacier in West Antarctica and implications for its retreat, Nature Geosci., 3, 468-472, 2010.

Joughin, I., Alley, R. B., and Holland, D. M.: Ice-Sheet Response to Oceanic Forcing, Science, 338, 1172-1176, 2012.

Lenaerts, J. T. M., Broeke, M. R. v. d., Berg, W. J. v. d., Meijgaard, E. v., and Munneke, a. P. K.: A new, high-resolution surface mass balance map of Antarctica(1979 – 2010) based on regional atmospheric climate modeling, Geophys. Res. Lett., 39, L04501, 2012.

Lenaerts, J. T. M., van den Broeke, M. R., van Wessem, J. M., van de Berg, W. J., van Meijgaard, E., van Ulft, L. H., and Schaefer, M.: Extreme Precipitation and Climate Gradients in Patagonia Revealed by High-Resolution Regional Atmospheric Climate Modeling, J Climate, 27, 4607-4621, 2014.

Ligtenberg, S. R. M., Helsen, M. M., and van den Broeke, M. R.: An improved semi-empirical model for the densification of Antarctic firn, Cryosphere, 5, 809-819, 2011.

Martinson, D. G., Stammerjohn, S. E., Iannuzzi, R. A., Smith, R. C., and Vernet, M.: Western Antarctic Peninsula physical oceanography and spatio–temporal variability, Deep Sea Research Part II Topical Studies in Oceanography, 55, 1964-1987, 2008.

McMillan, M., Shepherd, A., Sundal, A., Briggs, K., Muir, A., Ridout, A., Hogg, A., and Wingham, D.: Increased ice losses from Antarctica detected by CryoSat-2, Geophys. Res. Lett., 41, 3899-3905, 2014.

Mengel, M. and Levermann, A.: Ice plug prevents irreversible discharge from East Antarctica, Nature Clim. Change, 4, 451-455, 2014.

Nakayama, Y., Schröder, M., and Hellmer, H. H.: From circumpolar deep water to the glacial meltwater plume on the eastern Amundsen Shelf, Deep Sea Research Part I: Oceanographic Research Papers, 77, 50-62, 2013.

Pritchard, H. D., Ligtenberg, S. R. M., Fricker, H. A., Vaughan, D. G., van den Broeke, M. R., and Padman, L.: Antarctic ice-sheet loss driven by basal melting of ice shelves, Nature, 484, 502-505, 2012.

Rignot, E., Bamber, J. L., Van den Broeke, M. R., Davis, C., Li, Y., Van de Berg, W. J., and Van

Meijgaard, E.: Recent Antarctic ice mass loss from radar interferometry and regional climate modelling, Nature Geosci., 1, 106-110, 2008.

Rignot, E., Casassa, G., Gogineni, P., Krabill, W., Rivera, A., and Thomas, R.: Accelerated ice discharge from the Antarctic Peninsula following the collapse of Larsen B ice shelf, Geophys. Res. Lett., 31, L18401, 2004.

Rignot, E., Jacobs, S., Mouginot, J., and Scheuchl, B.: Ice Shelf Melting Around Antarctica, Science, 341, 266-270, 2013.

Rignot, E., Mouginot, J., and Scheuchl, B.: Antarctic grounding line mapping from differential satellite radar interferometry, Geophys. Res. Lett., 38, 2011.

Scambos, T. A., Bohlander, J. A., Shuman, C. A., and Skvarca, P.: Glacier acceleration and thinning after ice shelf collapse in the Larsen B embayment, Antarctica, Geophys. Res. Lett., 31, L18402, 2004.

Scheuchl, B.: MEaSUREs InSAR-based Ice Velocity of the Amundsen Sea Embayment. In: NASA DAAC at the National Snow and Ice Data Center, Boulder, Colorado USA, 2013.

Thomas, R., Rignot, E., Kanagaratnam, P., Krabill, W., and Casassa, G.: Force-perturbation analysis of Pine Island Glacier, Antarctica, suggests cause for recent acceleration, Annals of Glaciology, Vol 39, 2005, 39, 133-138, 2004.

van Wessem, J. M., Reijmer, C. H., Morlighem, M., Mouginot, J., Rignot, E., Medley, B., Joughin, I., Wouters, B., Depoorter, M. A., Bamber, J. L., Lenaerts, J. T. M., van de Berg, W. J., van den Broeke, M. R., and van Meijgaard, E.: Improved representation of East Antarctic surface mass balance in a regional atmospheric climate model, J Glaciol, 60, 761-770, 2014.

van Wessem, J. M., Ligtenberg, S. R. M., Reijmer, C. H., van de Berg, W. J., van den Broeke, M. R., Barrand, N. E., Thomas, E. R., Turner, J., Wuite, J., Scambos, T. A., and van Meijgaard, E.: The modelled surface mass balance of the Antarctic Peninsula at 5.5 km horizontal resolution, The Cryosphere, 10, 271-285, 2016.

Vaughan, D. G., Marshall, G. J., Connolley, W. M., Parkinson, C., Mulvaney, R., Hodgson, D. A., King, J. C., Pudsey, C. J., and Turner, J.: Recent rapid regional climate warming on the Antarctic Peninsula, Climatic change, 60, 243-274, 2003.

Wouters, B., Martin-Espanol, A., Helm, V., Flament, T., van Wessem, J. M., Ligtenberg, S. R. M., van den Broeke, M. R., and Bamber, J. L.: Dynamic thinning of glaciers on the Southern Antarctic Peninsula, Science, 348, 899-903, 2015.

Young, D. A., Wright, A. P., Roberts, J. L., Warner, R. C., Young, N. W., Greenbaum, J. S., Schroeder, D. M., Holt, J. W., Sugden, D. E., and Blankenship, D. D.: A dynamic early East Antarctic Ice Sheet suggested by ice-covered fjord landscapes, Nature, 474, 72-75, 2011.

Zwally, H., Giovinetto, M., Beckley, M., and Saba, J.: http://icesat4.gsfc.nasa.gov/cryo_data/ant_grn_drainage_systems.php, 2012.